PAPER

Check for updates

Effects of calcination and reduction temperature on the properties of Ni-P/SiO$_2$ and Ni-P/Al$_2$O$_3$ and their hydrodenitrogenation performance†

Mingqiang Shao, [ID] [ab] Haitao Cui,*[a] Shaoqing Guo,[c] Liangfu Zhao[a] and Yisheng Tan[a]

A series of SiO$_2$-supported and γ-Al$_2$O$_3$-supported nickel phosphides were prepared by temperature-programmed reduction (TPR) with different calcination and reduction temperatures. The prepared catalysts were characterized by XRD, BET, H$_2$-TPR, CO titration and HRTEM. The crystal phase and CO uptake content were influenced by calcination and reduction temperature. The catalytic performance of various catalysts was tested in quinoline hydrodenitrogenation and exhibited considerable differences. The quinoline HDN activity of SiO$_2$-supported nickel phosphides decreases with increase of calcination and reduction temperature. In contrast to SiO$_2$-supported samples, the ability to remove nitrogen of γ-Al$_2$O$_3$-supported samples increases with reduction temperature.

Introduction

Nickel phosphides as novel hydrotreating catalysts have received much attention.[1–3] They are widely investigated in hydrodesulfurization (HDS), hydrodenitrogenation (HDN) and hydrodeoxygenation (HDO), and exhibit special catalytic activity. The excellent catalytic activity is attributed to the ensemble and ligand effects.[4,5] In comparison with conventional sulfided catalysts, nickel phosphide catalysts show higher HDS and HDN activity.[6,7] For example, Sawhill *et al.* observed that Ni$_2$P/SiO$_2$ catalysts were approximately 15 and 3.5 times more active than conventional sulfided Mo/SiO$_2$ and Ni-Mo/SiO$_2$ catalysts in thiophene HDS.[8] SiO$_2$ and Al$_2$O$_3$ are widely used as supports in a variety of studies. Nevertheless, nickel phosphide catalysts supported on SiO$_2$ and Al$_2$O$_3$ exhibit very different catalytic activity in HDN and HDS.[9] Moreover, when Al$_2$O$_3$ is used as a support, more phosphide is used to produce Ni$_2$P because phosphide reacts with aluminum to form AlPO$_4$.

Some researchers obtained highly active nickel phosphide catalysts with different method at low pretreatment temperature. For example, PH$_3$ was used to form Ni$_2$P and the particle size of Ni$_2$P is similar to initial NiO.[10] Though nickel phosphide catalysts with various preparation methods are obtained, the most widely used method is temperature-programmed

reduction (TPR).[11] The method of TPR includes dry, calcination, reduction and passivation. In fact, every step above exerts a certain extent of influence on the catalytic activity. Wang *et al.* observed that Ni$_2$P/SiO$_2$ suffered from calcination exhibited lower HDN activity than uncalcined catalysts.[12] They attributed the low HDN activity to the less amount of Ni^0 caused by calcination, leading to low hydrogenation ability. Alexander and Kevin found that the passivated Ni$_2$P/SiO$_2$ possesses less CO uptake content after secondary reduction.[13] It is suggested that the catalyst suffered from sintering or reconstruction during the secondary reduction.

The commonly characterized means include XRD, H$_2$-TPR, TEM, CO titration and so on. H$_2$-TPR was a common and important characterization means, which could provide the information about the species types and reducibility of nickel phosphides. Generally, most researchers perform H$_2$-TPR experiments with heating rate of 10 °C min^{-1} or so to study the basic property of nickel phosphide catalysts.[14,15] However, the heating rate during catalytic test is usually 1 °C min^{-1} or so. Furthermore, the different heating rate may provide different reduction curves.[11] Consequently, the heating rate during characterization in line with test condition may provide more accurate and useful information. Up to now, heating rate of 1 °C min^{-1} is few reported during H$_2$-TPR characterization of nickel phosphides. In our study, heating rate of 1 °C min^{-1}, 3 °C min^{-1}, 10 °C min^{-1} were all investigated. Previously, Rodriguez *et al.* performed time resolved XRD experiments for Ni$_2$P/SiO$_2$ and explicitly explained the transformation way of Ni$_2$P precursors at ramp rate of 15 °C min^{-1}.[16] However, the influence of specific reduction temperature on the catalytic activity has not been investigated. The phenomenon observed at high heating rate of 15 °C min^{-1} is also a great difference from fact experimental condition at 1 °C min^{-1}.

[a]Institute of Coal Chemistry, Chinese Academy of Sciences, Taiyuan 030001, People's Republic of China. E-mail: cuiht@sxicc.ac.cn

[b]Graduate University of the Chinese Academy of Sciences, Beijing 100039, People's Republic of China

[c]Taiyuan University of Science and Technology, Taiyuan 030024, People's Republic of China

Experimental

Catalyst preparation

Precursors of 30 wt% nickel phosphide supported on SiO_2 were prepared with Ni and P atomic ratio of 1.25. This atomic ratio was proved to be optimal for quinoline HDN under the currently experimental conditions. Specifically, 3 g $NH_4H_2PO_4$ and 9.2 g $Ni(NO_3)_2 \cdot 6H_2O$ was added into 100 mL deionized water and then adjusted the pH to 2–3 by HNO_3. Subsequently, 10 g SiO_2 was poured into the above solution, stirring at 80 °C for 4 h. The samples were dried at 120 °C overnight and calcined at 440, 500, 560, 620 °C respectively for 5 h. TPR method was used to reduce the precursors. Each precursor was heated from room temperature to 560, 650 or 750 °C at a rate of 1 °C min^{-1} with a 50 mL min^{-1} H_2. Nickel phosphide catalysts were passivated with 0.5 vol% O_2/N_2 at room temperature for 6 h. The resulting catalysts were denoted as Ni-P_x^y/SiO_2, where x represents calcination temperature and y represents reduction temperature.

Samples of 30 wt% nickel phosphide supported on Al_2O_3 were prepared with Ni and P atomic ratio of 1.4. The synthesized steps were similar to Ni-P_x^y/SiO_2. And the obtained catalysts were also denoted as Ni-P_x^y/Al_2O_3.

Characterization method

A Rigaku D/max-2500 apparatus was used to carry out XRD experiments with a step of 4° s^{-1} over the 2θ range of 10–80°. The specific surface area was obtained on a Tristar-3020 and calculated on the basis of the BET isothermal equation. H_2 temperature programmed reduction (H_2-TPR) was performed using a Quantachrome ChemBET Pulsar TPR/TPD instrument equipped with a thermal conductivity detector (TCD). A sample (≈ 0.03 g) was firstly dried at 400 °C for 2 h in flowing He (50 mL min^{-1}). Subsequently, the sample was cooled to 80 °C and the He was changed into H_2/Ar. Finally, when the TCD signal reached stable reduction was conducted at a heating rate of 1, 3 and 10 °C min^{-1} in H_2/Ar (75 mL min^{-1}). The hydrogen consumption was determined by a TCD. Before detection, the gas was passed through a cold trap. A cold trap filled with a mixture of liquid nitrogen and acetone was employed to remove the produced water. Carbon monoxide (CO) uptakes over the samples were by a pulse injection method on a Quantachrome ChemBET Pulsar TPR/TPD instrument to estimate the content of active sites on the catalysts. Prior to injection of CO, the samples (0.25 g, 20–40 mesh) was firstly reduced in H_2/Ar (60 mL min^{-1}) at 450 °C for 2 h and then cooled to 30 °C in He (60 mL min^{-1}). Pulses of CO (50 μL, 10% CO/He) were injected in a He carrier until stable of the peak. A JEOL JEM-2100 F apparatus was used to obtain the transmission electron microscopy (HRTEM) image. The reduction samples were placed in ethanol with an ultrasonic dispersion for 1 hour and deposited on a Cu grid, and then the samples were dried at room temperature overnight. Determination of Ni and P contents was carried out using an ICP method with JY/T 015-1996 apparatus. Lewis and Brønsted acid density were determined by pyridine adsorption infrared (Py-IR) means using a Thermo Nicolet-380 apparatus. The corresponding samples (≈ 15 mg) were pressed into thin wafers and evacuated *in situ* under vacuum at 300 °C for 2 h (10^{-2} Pa) and then cooled to room temperature and collected the spectra of samples. After that, pyridine was dosed into the cell for 20 min. The sample was heated to 100 °C and kept for 30 min and then cooled to 40 °C and collected the spectra. Similarly, spectra treated at 200 °C was also obtained.

HDN catalytic test

Quinoline HDN test was performed. The quinoline HDN test of Ni-P/SiO_2 and Ni-P/γ-Al_2O_3 catalysts was conducted in a fixed-bed reactor with a mixture of 5000 ppm quinoline in decalin. 1 g passivated catalysts in 10–20 mesh size were loaded into the reaction tube. Prior to the catalytic test, the passivated catalysts were reduced in a 50 mL min^{-1} H_2 flow at 450 °C for 2 h. After that, the temperature was cooled to 360 °C. The quinoline solution was pumped into the fixed-bed reactor with a 3 g h^{-1} flow. The H_2/feed volumetric ratio was 1000 and H_2 pressure was 4 MPa.

The collected products after 12 h were qualitatively analyzed by an Agilent-5975C gas chromatograph-mass spectrometer and quantitatively analyzed by a Huaai 9560 gas chromatograph. To examine the stability of the Ni-P_x^{560}/SiO_2 and Ni-P_x^{750}/Al_2O_3 ($x = 440, 500, 560, 620$), the corresponding products were analyzed at time intervals of 24 h for a total time of 192 h.

The HDN conversion (HDN_C) of quinoline over the catalysts was expressed by the following equation:

$$HDN_C(\%) = \frac{n_{PB} + n_{PCH} + n_{PCHE}}{n_Q + \sum n_i}$$

where n_Q, n_{PCHE}, n_{OPA}, n_{PB}, and n_{PCH} represents the quinoline, propylcyclohexene, *ortho*-propylaniline, propylbenzene and propylcyclohexane concentration collected in the products, respectively. $\sum n_i$ represents the sum of all products concentration produced from quinoline, including 1,2,3,4-tetrahydroquinoline (THQ_1), 5,6,7,8-tetrahydroquinoline (THQ_5), decahydroquinoline (DHQ), *ortho*-propylaniline (OPA), propylbenzene (PB), propylcyclohexene (PCHE) and propylcyclohexane (PCH).

From the HDN conversion values, the turnover frequencies (TOFs) were calculated according to:

$$TOF(h^{-1}) = \frac{F_{A0}(\mu mol\ h^{-1}) \times HDN_C}{m(g) \times chemisorption\ uptake(\mu mol\ g^{-1})} \quad (1)$$

where F_{A0} is the molar flow of the quinoline feed (μmol h^{-1}).

Rate constants were calculated considering a first order kinetic by the following eqn (2):[17,18]

$$k(mol\ kg^{-1}\ h^{-1}) = -\frac{F_{A0}}{M}\ln(1 - HDN_C) \quad (2)$$

where k is the rate constant (mol kg^{-1} h^{-1}), F_{A0} the molar flow of the quinoline feed (mol h^{-1}), M the weight of catalysts (kg), HDN_C the denitrogenation conversion of quinoline.

Results and discussion

XRD patterns of SiO_2-supported and γ-Al_2O_3-supported nickel phosphides are given in Fig. 1. For SiO_2-supported nickel

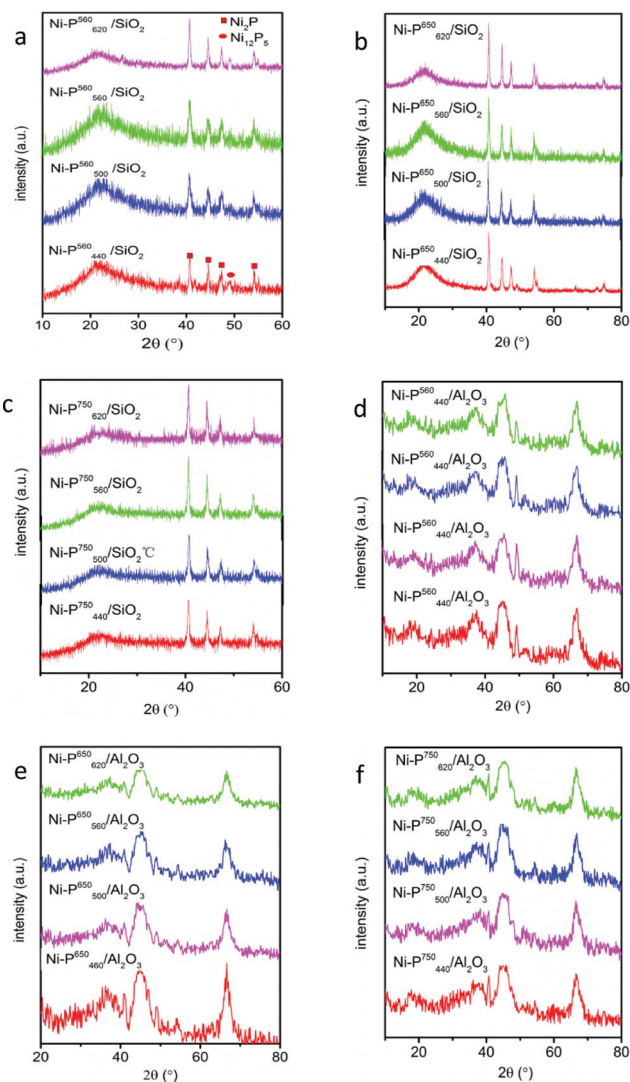Fig. 1 XRD patterns of different SiO_2-supported nickel phosphides reduced at (a) 560 °C, (b) 650 °C, (c) 750 °C and different γ-Al_2O_3-supported nickel phosphides reduced at (d) 560 °C, (e) 650 °C, (f) 750 °C.

phosphides, the broad peak ($\approx 21°$) is attributed to SiO_2 (PDF#27-0605). At reduction temperature of 560 °C, diffraction peaks assigned to $Ni_{12}P_5$ (PDF#22-1190) and Ni_2P (PDF#3-953) both appeared, and the main crystal phase is Ni_2P rather than $Ni_{12}P_5$. With increasing reduction temperature to 650 and 750 °C, only diffraction peak of Ni_2P is observed. For Ni-P/γ-Al_2O_3, the broad peaks ($\approx 45°$, 67°) are attributed to γ-Al_2O_3 (PDF#29-0063). It is shown that mere diffraction peak of $Ni_{12}P_5$ appeared at reduction temperature of 560 °C. But $Ni_{12}P_5$ and Ni_2P are observed at 650 and $Ni_{12}P_5$ diffraction peak became weak at 750 °C. It is also seen that the diffraction intensity of Ni_2P increased with calcination temperature at the same reduction temperature for Ni-P/SiO_2, indicating that the particle size increased with calcination temperature. XRD characterization of Ni-P$_{440}$/SiO_2 reduced at 460 and 520 °C was also performed and the result was presented in Figure S1.† It is observed that at reduction temperature of 460 °C, peak assigned

to $Ni_{12}P_5$ appeared. Up to 520 °C, peak attributed to Ni_2P was also detected. However, in the previous report, crystal phase of $Ni_{12}P_5$ appears at 550 °C and Ni_2P begins to form at 600 °C, while in our study the corresponding crystal was detected at lower temperature.[8]

The specific surface area (S_{BET}) of SiO_2-supported and γ-Al_2O_3-supported nickel phosphides was presented in Table 1 and their variation tendency of S_{BET} shows similar. The S_{BET} decreased as the reduction temperature increased for the samples with certain calcination temperature. For the sample with certain reduction temperature, the S_{BET} also decreased with increasing the calcination temperature. By increasing calcination and reduction temperature, crystal phase suffered from sintering and particle size became larger, leading to diminish of S_{BET}.

CO titration results are presented in Table 1. The CO uptake content declined as calcination temperature increased on account of growth of particle for both SiO_2 and γ-Al_2O_3-supported catalysts with determinate reduction temperature.

There are two aspects causing the decline of CO uptake content with increasing the reduction temperature. On one side, transformation of crystal phase occurred during reduction process. For example, both $Ni_{12}P_5$ and Ni_2P existed for Ni-P^{560}/SiO_2. While only Ni_2P was detected for Ni-P^{650}/SiO_2. On the other side, particle size tends to become larger.

H_2-TPR patterns of SiO_2-supported and γ-Al_2O_3-supported nickel phosphides are presented in Fig. 2. H_2-TPR patterns obtained at heating rate of 10 °C min^{-1} are shown in Fig. 2a and b. The two broad peaks at about 570 and 660 °C are assigned to reduction of nickel species and P–O bond for Ni-P/SiO_2. For

Table 1 Physical and chemical properties of different SiO_2-supported nickel phosphides and γ-Al_2O_3-supported nickel phosphides

Samples	S_{BET} (m^2 g^{-1})	CO uptake (µmol g^{-1})
Ni-P$_{440}^{560}$/SiO_2	262	36
Ni-P$_{500}^{560}$/SiO_2	257	36
Ni-P$_{560}^{560}$/SiO_2	253	35
Ni-P$_{620}^{560}$/SiO_2	250	32
Ni-P$_{440}^{650}$/SiO_2	257	19
Ni-P$_{500}^{650}$/SiO_2	253	18
Ni-P$_{560}^{650}$/SiO_2	250	18
Ni-P$_{620}^{650}$/SiO_2	247	17
Ni-P$_{440}^{750}$/SiO_2	252	16
Ni-P$_{500}^{750}$/SiO_2	249	16
Ni-P$_{560}^{750}$/SiO_2	248	14
Ni-P$_{620}^{750}$/SiO_2	247	14
Ni-P$_{440}^{560}$/Al_2O_3	182	174
Ni-P$_{500}^{560}$/Al_2O_3	180	172
Ni-P$_{560}^{560}$/Al_2O_3	178	168
Ni-P$_{620}^{560}$/Al_2O_3	174	163
Ni-P$_{440}^{650}$/Al_2O_3	180	121
Ni-P$_{500}^{650}$/Al_2O_3	177	118
Ni-P$_{560}^{650}$/Al_2O_3	175	113
Ni-P$_{620}^{650}$/Al_2O_3	173	109
Ni-P$_{440}^{750}$/Al_2O_3	178	63
Ni-P$_{500}^{750}$/Al_2O_3	176	62
Ni-P$_{560}^{750}$/Al_2O_3	174	60
Ni-P$_{620}^{750}$/Al_2O_3	172	58

Ni-P/γ-Al$_2$O$_3$, the peak becomes wider resulting from strong interaction between phosphide and γ-Al$_2$O$_3$. In the case of Ni-P$_{560}$/γ-Al$_2$O$_3$ and Ni-P$_{620}$/γ-Al$_2$O$_3$, reduction still occurs beyond 800 °C because of the existence of AlPO$_4$.[19] However, no obvious reduction peak is seen for Ni-P$_{440}$/γ-Al$_2$O$_3$ and Ni-P$_{500}$/γ-Al$_2$O$_3$. Fig. 2c and d show the H$_2$-TPR patterns obtained at heating rate of 3 °C min^{-1}. It is seen that the peak shape is similar to the patterns obtained at heating rate of 10 °C min^{-1}. Nevertheless, the peaks of both SiO$_2$-supported and γ-Al$_2$O$_3$-supported nickel phosphides were shifted to lower temperature. In the case of Ni-P/SiO$_2$, reduction was completed at approximately 620 °C. Fig. 2e and f show the H$_2$-TPR patterns obtained at heating rate of 1 °C min^{-1}. It is seen that the peaks shifted to lower temperature. In addition, only single peak ($\approx$ 500 °C) was observed for Ni-P/SiO$_2$. Reduction was almost finished at

560 °C. In addition, for the samples reduced at 10 °C min^{-1} the amount of H$_2$ consumed was contrasted with the theoretical amounts of H$_2$ needed to form the phosphide phases in each catalyst. The calculated results were listed in Tables S1 and S2.† According to Tables S1 and S2,† the SiO$_2$ and Al$_2$O$_3$-supported catalysts both shown lower consumption than the theoretical value. Furthermore, for Al$_2$O$_3$-supported catalysts the molar ratio of true consumption of H$_2$ to theoretical consumption of H$_2$ was lower than the SiO$_2$-supported catalysts. For SiO$_2$-supported catalysts, P$_x$O$_y$ could be produced, which was not able to be reduced. However, for Al$_2$O$_3$-supported catalysts a large amount of AlPO$_4$ was also produced but P$_x$O$_y$.[8]

Quinoline HDN catalytic test

Catalytic test with a variety of SiO$_2$-supported and γ-Al$_2$O$_3$-supported nickel phosphides was carried out and results are presented in Table 2. Apparently, it is seen that there are considerable HDN activity difference between SiO$_2$-supported and γ-Al$_2$O$_3$-supported nickel phosphides. In the case of Ni-P/SiO$_2$, the highest activity almost reaches 100%. While the optimal catalyst only reaches 57.8% for Ni-P/γ-Al$_2$O$_3$. The HDN activity decreased with increasing calcination and reduction temperature for SiO$_2$-supported nickel phosphides. Obviously, in comparison with reduction temperature, calcination temperature exerts greater influence on catalytic HDN activity. For example, the HDN conversion of Ni-P$_{440}$/SiO$_2$ drops from 99.2% to 96.4% as the reduction temperature increased. The HDN conversion drops from 99.2% to 83.8% with increasing the calcination temperature for Ni-P^{560}/SiO$_2$. In the case of Ni-P/
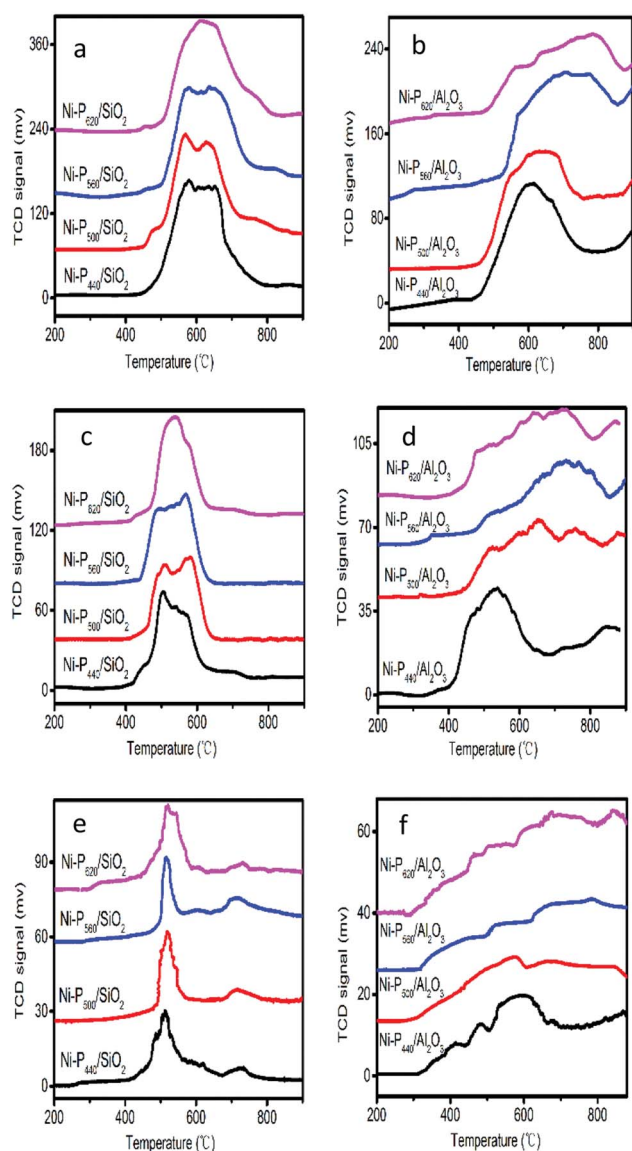

Fig. 2 H$_2$-TPR patterns of different SiO$_2$-supported nickel phosphides at heating rate of (a) 10 °C min^{-1}, (c) 3 °C min^{-1}, (e) 1 °C min^{-1} and different γ-Al$_2$O$_3$-supported nickel phosphides at heating rate of (b) 10 °C min^{-1}, (d) 3 °C min^{-1}, (f) 1 °C min^{-1}.

Table 2 Quinoline HDN conversion, TOF, and k of different (a) SiO$_2$-supported nickel phosphides and (b) γ-Al$_2$O$_3$-supported nickel phosphides

Samples	HDN$_C$ (%)	TOF (h^{-1})	k (mol kg^{-1} h^{-1})
Ni-P$_{440}$^{560}/SiO$_2$	99.4	2.14	0.40
Ni-P$_{500}$^{560}/SiO$_2$	95.3	2.05	0.24
Ni-P$_{560}$^{560}/SiO$_2$	89.1	1.98	0.17
Ni-P$_{620}$^{560}/SiO$_2$	81.4	1.96	0.13
Ni-P$_{440}$^{650}/SiO$_2$	98.6	4.02	0.33
Ni-P$_{500}$^{650}/SiO$_2$	93.7	4.02	0.21
Ni-P$_{560}$^{650}/SiO$_2$	86.7	3.74	0.16
Ni-P$_{620}$^{650}/SiO$_2$	83.2	3.78	0.14
Ni-P$_{440}$^{750}/SiO$_2$	96.4	4.66	0.26
Ni-P$_{500}$^{750}/SiO$_2$	91.3	4.42	0.19
Ni-P$_{560}$^{750}/SiO$_2$	79.3	4.38	0.13
Ni-P$_{620}$^{750}/SiO$_2$	78.3	4.33	0.12
Ni-P$_{440}$^{560}/Al$_2$O$_3$	16.9	0.075	0.014
Ni-P$_{500}$^{560}/Al$_2$O$_3$	15.6	0.067	0.013
Ni-P$_{560}$^{560}/Al$_2$O$_3$	14.7	0.068	0.012
Ni-P$_{620}$^{560}/Al$_2$O$_3$	12.8	0.061	0.011
Ni-P$_{440}$^{650}/Al$_2$O$_3$	33.5	0.214	0.032
Ni-P$_{500}$^{650}/Al$_2$O$_3$	32.3	0.211	0.031
Ni-P$_{560}$^{650}/Al$_2$O$_3$	31.9	0.208	0.030
Ni-P$_{620}$^{650}/Al$_2$O$_3$	31.6	0.209	0.029
Ni-P$_{440}$^{750}/Al$_2$O$_3$	58.6	0.720	0.068
Ni-P$_{500}$^{750}/Al$_2$O$_3$	57.3	0.715	0.066
Ni-P$_{560}$^{750}/Al$_2$O$_3$	54.3	0.700	0.061
Ni-P$_{620}$^{750}/Al$_2$O$_3$	52.1	0.695	0.057

γ-Al$_2$O$_3$, the variation tendency of HDN activity is not same as Ni-P/SiO$_2$. High calcination temperature is adverse to the catalyst, resulting in drop of the HDN conversion. While in contrast to Ni-P/SiO$_2$, high reduction temperature promotes the HDN activity of Ni-P/γ-Al$_2$O$_3$. In addition, reduction temperature imposes greater influence on catalytic HDN activity. For example, the HDN activity of Ni-P$_{440}$/Al$_2$O$_3$ was improved from 16.9% to 57.8% as the reduction temperature increased. The HDN conversion drops from 16.9% to 12.8% with increasing the calcination temperature for Ni-P^{560}/Al$_2$O$_3$.

The particle size tends to aggravate and becomes larger with increasing the calcination temperature for SiO$_2$-supported and Al$_2$O$_3$-supported nickel phosphides, leading to less exposure of active site. Here, the result of CO titration proved this. The CO uptake amount decreased with increasing the calcination temperature. In theory, HRTEM characterization can also find the difference resulted from calcination temperature. However, the distribution of catalyst particle is wide and the statistical result is not accurate (see Fig. S2†). For the sample with certain calcination temperature, the catalytic activity declined as the reduction temperature increased. According to H$_2$-TPR characterization of heating rate of 1 °C min^{-1}, it was found that the reduction of catalyst was nearly completed at 560 °C. Therefore, high reduction temperature not only no longer promotes the reducibility but also facilies the growth of particle. In the case of Ni-P/γ-Al$_2$O$_3$, the opposite tendency was observed compared with Ni-P/SiO$_2$. The HDN conversion dramatically increased with the reduction temperature. From H$_2$-TPR characterization of heating rate of 1 °C min^{-1}, the reduction still occurs beyond 750 °C. From XRD characterization, only Ni$_{12}$P$_5$ was produced at 560 °C, which was not as active as Ni$_2$P.[20] As reduction temperature increased, highly active Ni$_2$P was generated. Up to 750 °C, the predominant crystal phase was Ni$_2$P instead of Ni$_{12}$P$_5$. It should be mentioned that the H$_2$-TPR of heating rate of 1 °C min^{-1} explicitly explain the different phenomena for the two sets of catalysts. While the usual characterization method with heating rate of 3, 10 °C min^{-1} or others, it could not provide the accurate information.

The effect of calcination temperature on HDN of Ni-P/SiO$_2$ is more evident in comparison with Ni-P/γ-Al$_2$O$_3$. It is considered that the interaction of SiO$_2$ with nickel phosphides is weaker than γ-Al$_2$O$_3$ with nickel phosphides. This cause aggravate of nickel phosphide particle with elevating the calcination temperature, leading to the decrease of HDN active site.

The TOF numbers of various catalysts at different calcination and reduction temperatures are calculated and presented in Table 2. For both SiO$_2$ and Al$_2$O$_3$-supported catalysts, TOFs were decreased with increasing the calcination temperature at certain reduction temperatures. Furthermore, TOFs increase with reduction temperature. However, the increasing extent was quite different. For example, for SiO$_2$-supported catalysts, the TOFs of Ni-P$_{440}$^{750}/SiO$_2$ was almost twice as much as that of Ni-P$_{440}$^{560}/SiO$_2$. While for Al$_2$O$_3$-supported catalyst, the TOFs of Ni-P$_{440}$^{750}/Al$_2$O$_3$ was nearly 10 times as much Ni-P$_{440}$^{560}/Al$_2$O$_3$. Many researchers reported that the active phase for both HDS and HDN is Ni$_2$P. According to XRD, for Ni-P^{560}/Al$_2$O$_3$ the crystal phase was Ni$_{12}$P$_5$. But for Ni-P^{750}/Al$_2$O$_3$, the main crystal phase was Ni$_2$P. This results in considerable difference between Ni-P^{560}/Al$_2$O$_3$ and Ni-P^{750}/Al$_2$O$_3$. Overall, the rate constants the rate constants exhibited similarly tendency with TOF numbers (Table 2).

Prior to the cleavage of the carbon–nitrogen bond of quinoline, hydrogenation of heterocyclic has to be finished owing to the high carbon–nitrogen bond strength. There are mainly several products, including PCH, PB, DHQ, THQ$_1$ and THQ$_5$ (Table 3). A little amount of Q was detected due to the equilibrium with THQ$_1$ and THQ$_5$.[21] PCHA and PCHE was not detected due to the easily denitrogenation, hydrogenation and isomerization over nickel phosphides.[22] The content of OPA was little, suggesting that the further reaction rate of OPA is faster than its formation rate. It is obvious that the predominant denitrogenation products is PCH rather than PB, which is similar to the result reported by Oyama *et al.*[23] Perot, G. and Ho, T. C. reported that the reaction of OPA is inhibited by THQ1, Q and other nitrogen-containing compounds, resulting in the intrinsically unfavorable of denitrogenation *via* OPA to PB.[21,24] According to the reaction network in Scheme 1, there

Table 3 Product distribution of quinoline HDN catalyzed over different calcination and reduction catalysts

Samples	Q	THQ$_1$	THQ$_5$	DHQ	OPA	PB	PCH	PB/PCH
Ni-P$_{440}$^{560}/SiO$_2$	0	0.14	0.28	0.37	0	7.09	92.13	0.0769
Ni-P$_{500}$^{560}/SiO$_2$	0.06	1.21	0.49	2.76	0.36	6.95	88.17	0.0788
Ni-P$_{560}$^{560}/SiO$_2$	0.08	3.47	1.54	7.41	0.32	6.47	80.72	0.0801
Ni-P$_{620}$^{560}/SiO$_2$	0.12	6.27	2.47	9.31	0.51	6.38	74.94	0.0851
Ni-P$_{440}$^{750}/Al$_2$O$_3$	0.26	13.72	3.58	23.13	1.51	3.47	54.34	0.0638
Ni-P$_{500}$^{750}/Al$_2$O$_3$	0.15	13.51	4.17	23.84	1.43	3.37	53.53	0.0629
Ni-P$_{560}$^{750}/Al$_2$O$_3$	0.09	14.46	4.31	24.89	1.46	3.41	51.38	0.0663
Ni-P$_{620}$^{750}/Al$_2$O$_3$	0.23	15.18	4.19	24.71	1.39	3.59	50.71	0.0709
Ni-P$_{440}$^{650}/SiO$_2$	0.06	0.42	0.27	0.56	0.07	7.28	91.32	0.0797
Ni-P$_{500}$^{650}/SiO$_2$	0.12	1.27	0.93	3.84	0.14	6.86	86.84	0.0790
Ni-P$_{560}$^{650}/SiO$_2$	0.08	4.14	1.43	7.36	0.27	6.59	80.12	0.0822
Ni-P$_{620}$^{650}/SiO$_2$	0.18	4.69	1.37	10.32	0.24	6.73	76.47	0.0871
Ni-P$_{440}$^{750}/SiO$_2$	0.07	1.36	0.64	1.39	0.17	7.16	89.23	0.0802
Ni-P$_{500}$^{750}/SiO$_2$	0.06	4.24	1.02	6.13	0.23	6.89	81.42	0.0816
Ni-P$_{560}$^{750}/SiO$_2$	0.18	4.63	2.41	13.14	0.36	6.12	73.16	0.0837
Ni-P$_{620}$^{750}/SiO$_2$	0.14	5.63	2.63	12.98	0.32	6.35	71.93	0.0882
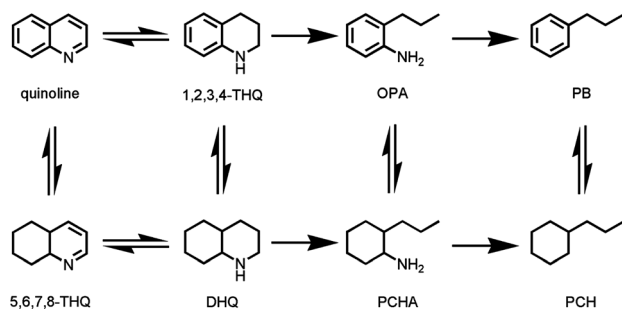
Scheme 1 HDN reaction network of quinoline.
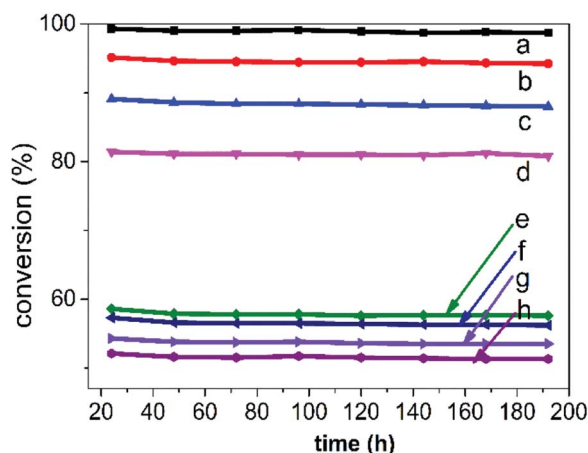
Fig. 3 HDN$_C$ of quinoline as a function of time. a, b, c, d, e, f, g and h represents Ni-P$_{440}^{560}$/SiO$_2$, Ni-P$_{500}^{560}$/SiO$_2$, Ni-P$_{560}^{560}$/SiO$_2$, Ni-P$_{620}^{560}$/SiO$_2$, Ni-P$_{440}^{750}$/Al$_2$O$_3$, Ni-P$_{500}^{750}$/Al$_2$O$_3$, Ni-P$_{560}^{750}$/Al$_2$O$_3$, Ni-P$_{620}^{750}$/Al$_2$O$_3$, respectively.

are mainly two HDN pathways, *via* OPA or *via* DHQ. For the first path of OPA, hydrogenation of OPA to PCHA is the rate determining step. For the second path of DHQ, the rate determining step is C–N bond cleavage of DHQ to PCHA. According to the product distribution of Table 3, the ratio of PB to PCH was all slightly increased with the calcination temperature at certain reduction temperature. It is considered that two reasons give rise to this result. From CO uptakes, the number of active sites decreased as the calcination temperature was increased, resulting in decline of hydrogenation activity of OPA to PCHA. Furthermore, the number of Bronsted acidity was also declined with increasing the calcination temperature (Table S3†). Bronsted acid could promote the C–N bond cleavage of PCHA. The Bronsted acid site was produced by hydroxyl group of phosphide. However, high calcination temperature causes condensation of hydroxyl group, resulting in decrease of Bronsted acidity.

HDN reaction network of quinoline.Stability of Ni-P$_x^{560}$/SiO$_2$ and Ni-P$_x^{750}$/Al$_2$O$_3$ (x = 440, 500, 560, 620) were examined and the products were analysed in 24 h intervals for 192 h. The results were presented in Fig. 3. Overall, there is little decline of catalytic activity during examined period, indicating the promising industrial perspective for this kind of catalyst. In fact, the HDN$_C$ of Ni-P$_{440}^{560}$/SiO$_2$, Ni-P$_{500}^{560}$/SiO$_2$, Ni-P$_{560}^{560}$/

SiO$_2$, Ni-P$_{620}^{560}$/SiO$_2$ catalysts falls 0.7, 0.9, 1.2, 0.7% in 192 h, respectively. The Ni-P$_{440}^{750}$/Al$_2$O$_3$, Ni-P$_{500}^{750}$/Al$_2$O$_3$, Ni-P$_{560}^{750}$/Al$_2$O$_3$, Ni-P$_{620}^{750}$/Al$_2$O$_3$ catalysts drops 1.7, 1.5, 1.9, 1.4% in 192 h, respectively. Although no evident drops were observed for both two set of catalysts, there were still some difference between them. It is considered that more coke deposition happened over Al$_2$O$_3$-supported catalysts, resulting in cover of active sites. The deactivation by coke is related to catalyst acidity, which the Al$_2$O$_3$-supported catalysts have higher amount of acidity than the SiO$_2$-supported catalysts from Py-IR results.

Conclusions

In comparison with γ-Al$_2$O$_3$-supported nickel phosphides, highly HDN active phase of Ni$_2$P was formed on SiO$_2$-supported nickel phosphides at lower reduction temperature.

From H$_2$-TPR, the peak was shifted towards lower temperature with decreasing the heating rate. The SiO$_2$-supported nickel phosphides were reduced absolutely at 560 °C. The reduction was still performed beyond 750 °C for γ-Al$_2$O$_3$-supported nickel phosphides.

The quinoline HDN active sites and conversion was reduced when the reduction temperature surpassed 560 °C for nickel phosphides supported on SiO$_2$. While the quinoline HDN active sites and conversion dramatically increased with increasing the reduction temperature for nickel phosphides supported on γ-Al$_2$O$_3$.

Conflicts of interest

There are no conflicts to declare.

Acknowledgements

References

1 S. T. Oyama and Y. K. Lee, *J. Phys. Chem. B*, 2005, **109**, 2109–2119.

2 Y. Y. Shu, Y. K. Lee and S. T. Oyama, *J. Catal.*, 2005, **236**, 112–121.

3 S. De, J. Zhang, R. Luque and N. Yan, *Energy Environ. Sci.*, 2016, **9**, 3314–3347.

4 P. Liu and J. A. Rodriguez, *J. Am. Chem. Soc.*, 2005, **127**, 14871–14878.

5 P. Liu, J. A. Rodriguez, T. Asakura, J. Gomes and K. Nakamura, *J. Phys. Chem. B*, 2005, **109**, 4575–4583.

6 M. Lu, A. Wang, X. Li, X. Duan, Y. Teng, Y. Wang, C. Song and Y. Hu, *Energy Fuels*, 2007, **21**, 554–560.

7 L. Zhang, W. Fu, Q. Yu, T. Tang, Y. Zhao, H. Zhao and Y. Li, *J. Catal.*, 2016, **338**, 210–221.

8 S. J. Sawhill, K. A. Layman, D. R. Van Wyk, M. H. Engelhard, C. Wang and M. E. Bussell, *J. Catal.*, 2005, **231**, 300–313.

9 A. I. d'Aquino, S. J. Danforth, T. R. Clinkingbeard, B. Ilic, L. Pullan, M. A. Reynolds, B. D. Murray and M. E. Bussell, *J. Catal.*, 2016, **335**, 204–214.

10 S. F. Yang, C. H. Liang and R. Prins, *J. Catal.*, 2006, **237**, 118–130.

11 V. T. da Silva, L. A. Sousa, R. M. Amorim, L. Andrini, S. J. A. Figueroa, F. G. Requejo and F. C. Vicentini, *J. Catal.*, 2011, **279**, 88–102.

12 W. Wang, X. Li, Z. C. Sun, A. J. Wang, Y. Y. Liu, Y. Y. Chen and X. P. Duan, *Appl. Catal., A*, 2016, **509**, 45–51.

13 A. L. Imbault and K. J. Smith, *Catal. Lett.*, 2016, **146**, 1886–1891.

14 J. Chen, S. Zhou, D. Ci, J. Zhang, R. Wang and J. Zhang, *Ind. Eng. Chem. Res.*, 2009, **48**, 3812–3819.

15 J. X. Chen, Y. Chen, Q. Yang, K. L. Li and C. C. Yao, *Catal. Commun.*, 2010, **11**, 571–575.

16 J. A. Rodriguez, J. Y. Kim, J. C. Hanson, S. J. Sawhill and M. E. Bussell, *J. Phys. Chem. B*, 2003, **107**, 6276–6285.

17 T. I. Koranyi, A. E. Coumans, E. J. M. Hensen, R. Ryoo, H. S. Kim, E. Pfeifer and Z. Kasztovszky, *Appl. Catal., A*, 2009, **365**, 48–54.

18 V. H. J. Debeer, G. C. A. Schuit, T. h. Van sintf, A. c. Van haand, M. W. J. Wolfs, J. F. Engelen and C. H. Amberg, *J. Catal.*, 1972, **27**, 357–363.

19 P. A. Clark and S. T. Oyama, *J. Catal.*, 2003, **218**, 78–87.

20 S. T. Oyama, X. Wang, Y. K. Lee, K. Bando and F. G. Requejo, *J. Catal.*, 2002, **210**, 207–217.

21 G. Perot, *Catal. Today*, 1991, 447–472.

22 M. Lu, A. Wang, X. Li, X. Duan, Y. Teng, Y. Wang, C. Song and Y. Hu, *Energy Fuels*, 2007, **21**, 554–560.

23 S. T. Oyama, X. Wang, Y. K. Lee and W. J. Chun, *J. Catal.*, 2004, **221**, 263–273.

24 T. C. Ho, *Catal. Rev.: Sci. Eng.*, 1988, **30**, 117–160.